Energy-bandwidth trade-off in all-optical photonic crystal microcavity switches

Heuck, Mikkel; Kristensen, Philip Trøst; Mørk, Jesper

Published in:
Optics Express

Link to article, DOI:
10.1364/OE.19.018410

Publication date:
2011

Document Version
Publisher's PDF, also known as Version of record

Energy-bandwidth trade-off in all-optical photonic crystal microcavity switches

Mikkel Heuck,* Philip Trøst Kristensen, and Jesper Mørk

DTU Fotonik, Department of Photonics Engineering, Technical University of Denmark, Oersteds Plads 343, DK-2800 Kgs. Lyngby, Denmark

*mheu@fotonik.dtu.dk

Abstract: The performance of all-optical switches is a compromise between the achievable bandwidth of the switched signal and the energy requirement of the switching operation. In this work we consider a system consisting of a photonic crystal cavity coupled to two input and two output waveguides. As a specific example of a switching application, we investigate the demultiplexing of an optical time division multiplexed signal. To quantify the energy-bandwidth trade-off, we introduce a figure of merit for the detection of the demultiplexed signal. In such investigations it is crucial to consider patterning effects, which occur on time scales that are longer than the bit period. Our analysis is based on a coupled mode theory, which allows for an extensive investigation of the influence of the system parameters on the switching dynamics. The analysis is shown to provide new insights into the ultrafast dynamics of the switching operation, and the results show optimum parameter ranges that may serve as design guidelines in device fabrication.

OCIS codes: (200.4560) Optical data processing; (160.5298) Photonic crystals.

References and links

1. M. Soljačić and J. D. Joannopoulos, "Enhancement of nonlinear effects using photonic crystals," Nature Mater. **3**, 211–219 (2004).
2. J. Y. Lee, L. H. Yin, G. P. Agraval, and P. M. Fauchet, "Ultrafast optical switching based on nonlinear polarization rotation in silicon waveguides," Opt. Express **18**, 11514–11523 (2010).
3. M. Waldow, T. Plotzing, M. Gottheil, M. Forst, and J. Bolten, "25 ps all-optical switching in oxygen implanted silicon-on-insulator microring resonator," Opt. Express **16**, 7693–7702 (2008).
4. C. Husko, A. De Rossi, S. Combré, Q. V. Tran, F. Raineri, and C. W. Wong, "Ultrafast all-optical modulation in GaAs photonic crystal cavities," Appl. Phys. Lett. **94**, 021111 (2009).
5. K. Nozaki, T. Tanabe, A. Shinya, S. Matsuo, T. Sato, H. Taniyama, and M. Notomi, "Sub-femtojoule all-optical switching using a photonic-crystal nanocavity," Nat. Photonics **4**, 477–483 (2010).
6. L. O'Faolain, D. M. Beggs, T. P. White, T. Kampfrath, K. Kuipers, and T. F. Krauss, "Compact optical switches and modulators based on dispersion engineered photonic crystals," IEEE Photon. J. **2**, 404–414 (2010).
7. O. Wada, "Recent progress in semiconductor-based photonic signal-processing devices," IEEE J. Sel. Top. Quantum Electron. **17**, 309–319 (2011).
8. P. A. Andrekson, H. Sunnerud, S. Oda, T. Nishitani, and J. Yang, "Ultrafast, atto-Joule switch using fiber parametric amplifier operated in saturation," Opt. Express **16**, 10956–10961 (2008).
9. J. Xu, X. Zhang, and J. Mørk, "Investigation of patterning effects in ultrafast SOA-based optical switches," IEEE J. Quantum Electron. **46**, 87–94 (2010).
10. J. B. Khurgin, "Performance of nonlinear photonic crystal devices at high bit rates," Opt. Lett. **30**, 643–645 (2005).

#149819 - $15.00 USD Received 1 Jul 2011; revised 8 Aug 2011; accepted 22 Aug 2011; published 6 Sep 2011

11. M. F. Yanik, S. Fan, M. Soljacic, and J. D. Joannopoulos, "All-optical transistor action with bistable switching in a photonic crystal cross-waveguide geometry," Opt. Lett. **28**, 2506–2508 (2003).
12. J. Bravo-Abad, S. Fan, S. G. Johnson, J. D. Joannopoulos, and M. Soljačić, "Modeling nonlinear optical phenomena in nanophotonics," J. Lightwave Technol. **25**, 2539–2546 (2007).
13. J. D. Joannopoulos, S. G. Johnson, J. N. Winn, and R. D. Meade, *Photonic Crystals, Molding the Flow of Light* (Princeton University Press, 2008)
14. H. M. Lai, P. T. Leung, K. Young, P. W. Barber, and S. C. Hill, "Time-independent perturbation for leaking electromagnetic modes in open systems with application to resonances in microdroplets," Phys. Rev. A **41**, 5187–5198 (1990).
15. J. Mørk, F. Öhmann, and S. Bischoff, "Analytical expression for the bit error rate of cascaded all-optical regenerators," Photon. Technol. Lett. **15**, 1479–1481 (2003).
16. R. W. Boyd, *Nonlinear Optics* (Academic Press, 2008)

1. Introduction

All-optical switches are expected to play a key role in increasing the bandwidth of future communication networks by replacing slower electronic components for certain signal processing tasks. Photonic crystal (PhC) membranes show great promise as a platform for such devices due to the possibility of designing high Q cavities with ultra small mode volumes and waveguides with highly tailorable dispersion characteristics [1]. They also have the advantage of being able to integrate many components on the same chip, which is an important device requirement. In order to make light fields interact and achieve all-optical switching it is necessary for the PhC material to have a nonlinear response. The switching operation is facilitated by using a control pulse to change the refractive index and/or gain of the material through the nonlinear interaction. This change alters the transmission for a signal pulse, and thus opens or closes the switch. Different physical phenomena may be responsible for the nonlinearity, but there is a general trend showing that very fast responses are also very weak and thus require large field intensities. This results in an energy-bandwidth trade-off, which means that larger bandwidths are only achievable at the cost of a larger energy consumption of the device. By using PhC cavities with large Q-values it is possible to achieve a large field enhancement, which reduces the energy requirement. However, it also limits the transmission of the cavity, and the increased photon lifetime causes patterning effects, which restrict the signal bandwidth. So again, there is a trade-off between energy consumption and bandwidth.

All-optical switching has been demonstrated using many different platforms and materials such as silicon waveguides [2] and micro rings [3], PhC cavities [4, 5] and Mach-Zender interferometers [6], semiconductor optical amplifiers [7], and parametric processes in fibers [8]. In many cases, these demonstrations only consider switching of a single pulse. In this work, we will define a figure of merit that applies to any type of switching device, and is suitable for evaluating the switching performance in high speed optical communication systems. In particular, we will include patterning effects, which arise when the control pulse affects succeeding signal pulses.

Previous work [9] has considered patterning effects in semiconductor optical amplifier based switches as well as the high bit rate performance of photonic crystal switches based on shifting the photonic band gap edge and an interferometric approach enhanced by the slow light property of photonic crystals [10]. Here, we consider a different type of device, which uses a cavity to enhance the light matter interaction. Our aim is to evaluate the limits of the operation speed set by the cavity alone, and therefore consider the instantaneous Kerr effect to be the only nonlinear interaction in the system. Since there are a large number of possible applications for a switching device, a single figure of merit does not quantify them all. Here, we shall consider demultiplexing of optical-time-division-multiplexed (OTDM) signals as a specific and important application example.

The coupled-mode-theory (CMT) model that we use to analyse the switching dynamics has

#149819 - $15.00 USD Received 1 Jul 2011; revised 8 Aug 2011; accepted 22 Aug 2011; published 6 Sep 2011

the advantage that it is not limited to a specific type of structure like a PhC, but applies to a broader range of systems that share a set of common properties. Furthermore, it is simple enough to allow an extensive parameter investigation, and despite its simplicity it has been shown to provide excellent agreement with full finite-difference-time-domain calculations (FDTD) [11, 12].

In the following section, we first describe the example system and the general model considered. Then, in Sec. 3, we investigate the simplest case of single pulse transmission through the switch. A figure of merit for the detection of different channels in an OTDM signal is introduced in Sec. 4, and in Secs. 5 and 6 we investigate the effects of a number of the system parameters on the switching dynamics. Our conclusions follow in Sec. 7.

2. Model

The PhC structure illustrated in Fig. 1(a) consists of high index rods with a dielectric constant, $\varepsilon_r = 12$, surrounded by air and has two input waveguides and two output waveguides coupled to a cavity at the center, similar to Ref. [11]. In Fig. 1(b), the parameters entering a CMT

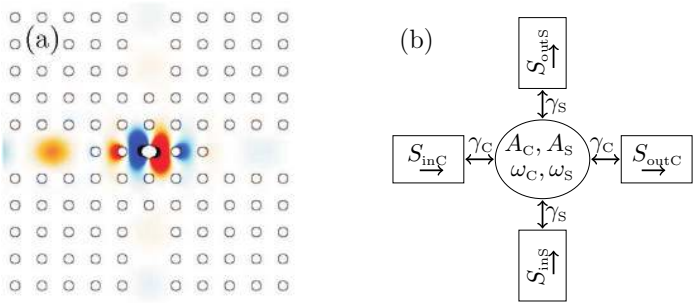

Fig. 1. (a) The switching structure investigated with a central cavity and two input and two output waveguides. An example of a steady state E_z-field distribution with inputs from the left and the bottom is overlaid on the structure. (b) CMT model of the structure in (a) with an illustration of the parameters entering Eqs. (1) and (2).

model of the same system are indicated. We will assume that the nonlinear response of the cavity is dominated by the Kerr effect. For the pulse widths considered here, this effect may be considered instantaneous.

The rod in the center of the structure in Fig. 1(a) has an elliptical shape, which results in two field modes that are denoted $A_i(t)$, where $i = \mathrm{S,C}$ is short for signal and control. We shall call them cavity mode S and cavity mode C. The fields in the waveguides are denoted $S_{\mathrm{inS,C}}(t)$ and $S_{\mathrm{outS,C}}(t)$ corresponding to the input and output waveguides. The resonance frequencies of the cavity modes are $\omega_{\mathrm{S,C}}$ and the coupling of light between the cavity modes and waveguides is described by the field decay rates $\gamma_{\mathrm{S,C}}$. The fields are normalized so that $|S_{\mathrm{in(out)S,C}}|^2 = P_{\mathrm{in(out)S,C}}$ is the power in the input (output) waveguides, and $|A_i|^2 = U_i$ is the energy in the cavity modes. These fields are the slowly varying envelopes, related to the total fields by $a_i(t) = A_i(t)\exp(-i\omega_{\mathrm{L}_i}t)$ and $s_i(t) = S_i(t)\exp(-i\omega_{\mathrm{L}_i}t)$, where ω_{L_i} are the carrier frequencies of the input fields. In the case where a signal beam is sent in through one waveguide and a control beam through another, the time evolution of the waveguide fields is governed by

#149819 - $15.00 USD Received 1 Jul 2011; revised 8 Aug 2011; accepted 22 Aug 2011; published 6 Sep 2011

the CMT equations [13]

$$\frac{dS_{\mathrm{outS}}}{dt} = -i\delta_{\mathrm{S}} S_{\mathrm{outS}} + i\frac{1}{\tau_{\mathrm{S}}}\left(\frac{P_{\mathrm{outS}}}{P_{\mathrm{SS}}} + 2\frac{P_{\mathrm{outC}}}{P_{\mathrm{SC}}}\right) S_{\mathrm{outS}} - \frac{1}{\tau_{\mathrm{S}}}(S_{\mathrm{outS}} - S_{\mathrm{inS}}) \tag{1}$$

$$\frac{dS_{\mathrm{outC}}}{dt} = -i\delta_{\mathrm{C}} S_{\mathrm{outC}} + i\frac{1}{\tau_{\mathrm{C}}}\left(\frac{P_{\mathrm{outC}}}{P_{\mathrm{CC}}} + 2\frac{P_{\mathrm{outS}}}{P_{\mathrm{CS}}}\right) S_{\mathrm{outC}} - \frac{1}{\tau_{\mathrm{C}}}(S_{\mathrm{outC}} - S_{\mathrm{inC}}). \tag{2}$$

Here, we have introduced the total lifetime of each cavity mode, $1/\tau_i = 2\gamma_i$, the detuning of the input fields from the cavity resonances, $\delta_i = \omega_i - \omega_{L_i}$, and the characteristic powers

$$\frac{1}{P_{ij}} = \frac{2}{\varepsilon_0 \varepsilon_{\mathrm{r}}^{\max} c}\frac{\omega_i}{c}\kappa_{ij} Q_i Q_j \chi_{\max}^{(3)}, \tag{3}$$

where $i, j = \mathrm{S,C}$. The parameters: ε_0, c, $\varepsilon_{\mathrm{r}}^{\max}$, $\chi_{\max}^{(3)}$, are the vacuum permittivity, the speed of light in vacuum, and the maximum values of the relative permittivity and third order susceptibility within the caviy. $Q_i = \omega_i \tau_i/2$ is the quality factor of cavity mode i, and κ_{ij} is a parameter describing the overlap of the fields within the active region of the cavity. For open systems with a finite quality factor the calculation of κ_{ij} is nontrivial and should be handled within the framework of non-hermitian differential equations [14]. Alternatively, expressions for the steady state powers, P_{outS} and P_{outC}, can be derived from Eqs. (1) and (2), and these may be used to fit results from FDTD calculations, whereby the values of κ_{ij} can be determined. This issue, however, is not the main focus of this work, so we choose values of κ_{ij} that result in characteristic powers, which are similar to the values in Ref. [11].

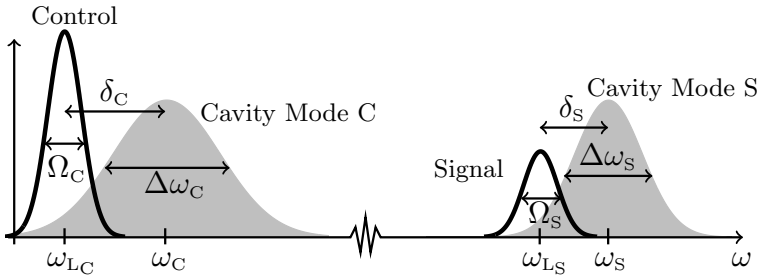

Fig. 2. Illustration of the power spectra of the signal and control as well as the Lorentzian transmission spectra of the cavity modes.

From the steady state solution of the linear part of Eqs. (1) and (2), it can be shown that the transmission spectra of the cavity modes are Lorentzians with a full width at half maximum (FWHM) of $\Delta\omega_i = 2/\tau_i$ [13]. Fig. 2 illustrates these transmission spectra as well as the spectra of the signal and control pulses and indicates the corresponding parameters. The FWHM of the pulses are denoted Ω_i. In a structure like the one shown in Fig. 1(a), where the waveguides for the signal and control are spatially separated, the Q-values of the modes can be controlled independently by placing a different number of extra rods adjacent to the cavity in the two waveguides. This turns out to be important, since the results in Sec. 5 will show that an optimum switching performance is achievable by using very different linewidths for the two modes. In Ref. [11] it was shown that changing Q by placing more rods next to the cavity does not significantly affect κ_{ij}, if the corresponding change in the field distributions in the center of the cavity is negligible. This justifies using $\Delta\omega_{\mathrm{S}}$ and $\Delta\omega_{\mathrm{C}}$ as independent parameters, which may be varied significantly in value.

#149819 - $15.00 USD Received 1 Jul 2011; revised 8 Aug 2011; accepted 22 Aug 2011; published 6 Sep 2011

In Eqs. (1) and (2) all the energy loss from the cavity modes is assumed to go into the waveguides. To be more general, the equations could have contained an extra loss term, $-\Gamma S_{\mathrm{outS,C}}$, where Γ would be the rate of energy loss due to out of plane scattering or absorption in the cavity. We neglect such a term here to keep the description as simple as possible. The second terms in Eqs. (1) and (2) describe the nonlinear shift in the resonance frequency of the cavity modes due to self- and cross phase modulation. By combining the first and second terms in Eq. (1), we may define a power dependent effective detuning

$$\delta_{\mathrm{S}}^{\mathrm{eff}} = \delta_{\mathrm{S}} - \frac{1}{\tau_{\mathrm{S}}}\left(\frac{P_{\mathrm{outS}}}{P_{\mathrm{SS}}} + 2\frac{P_{\mathrm{outC}}}{P_{\mathrm{SC}}}\right). \tag{4}$$

The operation principle of the switch is easily understood from Fig. 2 and Eqs. (1) and (4). The injected control pulse redshifts the transmission spectrum of cavity mode S, which increases its overlap with the signal spectrum and opens the switch.

An important strength of the CMT model is that it applies to any system, which consists of a two-mode cavity with Lorentzian transmission spectra and no cross-talk between the signal and control waveguides. For the system considered here, we use parameter values that are similar to those in [11], and they are: $\omega_{\mathrm{S}} = 2.344\ c/a$, $\omega_{\mathrm{C}} = 2.231\ c/a$, $\kappa_{\mathrm{SS}} = 0.0943$, $\kappa_{\mathrm{CC}} = 0.105$, $\kappa_{\mathrm{SC}} = 0.0312$, and $\kappa_{\mathrm{CS}} = 0.0343$, where a is the lattice constant of the PhC structure.

3. Transmission of a Single Signal Pulse

In order to understand the dynamics of systems described by Eqs. (1) and (2), we start by considering the case of a single signal pulse in which case there is no coupling term in the equations. The very short pulses employed in OTDM signals typically originate from mode-locked lasers, which emit pulses with a shape that is well approximated by a Gaussian function

$$P_{\mathrm{inS}}(t) = P_{\mathrm{inS}}^{0} \exp\left[-\ln(2)\left(\frac{2t}{\Delta t_{\mathrm{S}}}\right)^{2}\right],$$

where Δt_{S} is the FWHM pulse width.

First, we consider the transition from a quasi steady state regime of very long pulses to the case of ultra short pulses, where the pulse bandwidth Ω_{S} is larger than the cavity linewidth $\Delta\omega_{\mathrm{S}}$. Although we will primarily focus on Gaussian pulses, it is more illustrative to use square pulses for this purpose, because the steady state appears as the limit of an infinitely long square pulse. While keeping the cavity linewidth constant, we have varied the peak power of the input pulse for different values of the pulse width. Fig 3(a) shows the ratio of output energy and pulse width as a function of the input power for different values of $\Delta\omega_{\mathrm{S}}/\Omega_{\mathrm{S}}$ for a square pulse. The steady state solution of Eq. (1) is also plotted (dashed red) and agrees well with the results in [11]. The steady state curve shows a characteristic bistable behavior with an intermediate unstable solution. When the pulse bandwidth is larger than the cavity linewidth, the output energy shows local extrema as a function of input power. The same behavior is observed for a Gaussian pulse (shown in Fig. 3(b)). The reason for the appearance of the local extrema is oscillations in the output power. To illustrate this point, Fig. 3(c) shows the input (black) and output (red) power corresponding to the local extrema indicated by green dots in Fig. 3(b). The oscillations reflect a purely linear phenomenon, which is most clearly illustrated by considering the solution of the linear part of Eq. (1) in the case of a step function input

$$P_{\mathrm{inS}}(t) = P_{\mathrm{inS}}^{0}\Theta(t), \quad \Theta(t) = \begin{cases} 1 & \text{for} \quad t \geq 0 \\ 0 & \text{for} \quad t < 0 \end{cases}.$$

#149819 - $15.00 USD Received 1 Jul 2011; revised 8 Aug 2011; accepted 22 Aug 2011; published 6 Sep 2011

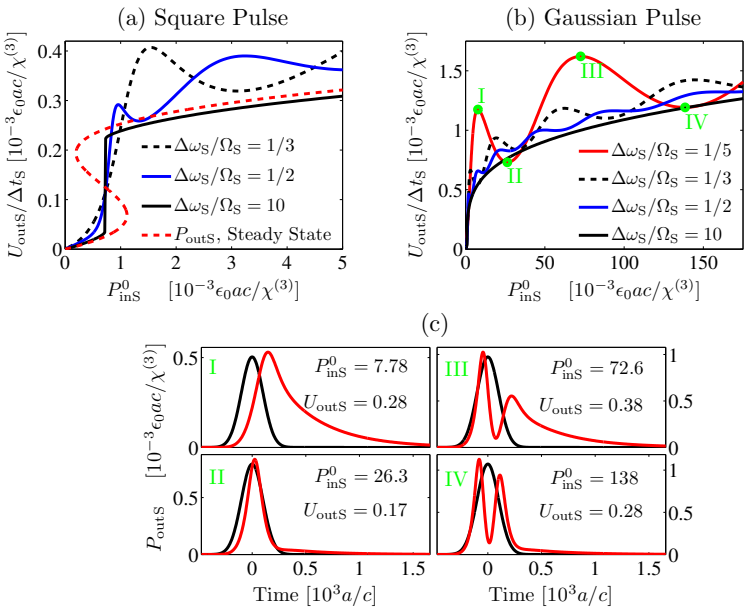

Fig. 3. (a) Ratio of output energy to input pulse width as a function of the input peak power for a square pulse. The different curves correspond to different pulse widths, while the cavity linewidth is fixed. The dashed red line shows the characteristic bistability curve found from the steady state solution of Eq. (1). (b) The same as (a), but for a Gaussian pulse. Notice the different scales on the P^0_{inS}-axis in (a) and (b). The green dots indicate local extrema in the output as a function of P^0_{inS}. (c) Input (black) and output (red) power of a Gaussian pulse with input powers corresponding to the green dots in (b). The curve of the input power has been scaled to be comparable to the output. The values of input power and output energy are given in units of $[10^{-3}\varepsilon_0 ca/\chi^{(3)}]$ and $[\varepsilon_0 a^2/\chi^{(3)}]$, respectively. The parameters in both (a), (b), and (c) are: $\Delta\omega_{\mathrm{S}} = 2.344\times10^{-3}c/a$ and $\delta_{\mathrm{S}} = 3\Delta\omega_{\mathrm{S}}$.

The output power can in this case be expressed analytically, and is given by

$$P_{\mathrm{outS}}(t) = P^0_{\mathrm{inS}}\frac{\Delta\omega_{\mathrm{S}}^2}{\Delta\omega_{\mathrm{S}}^2+4\delta_{\mathrm{S}}^2}\left[1+\exp\left(-\Delta\omega_{\mathrm{S}}t\right)-2\exp\left(-\Delta\omega_{\mathrm{S}}t/2\right)\cos\left(\delta_{\mathrm{S}}t\right)\right]\Theta(t), \qquad (5)$$

which oscillates with a period given by the detuning, δ_{S}. The physical origin of the oscillations is a transient interference beating between the incoming pulse oscillating at $\omega_{\mathrm{L_S}}$ and the excited cavity mode oscillating at ω_{S}. In the top left graph of Fig. 3(c) the oscillation period is $\sim$4 times the pulse width, and the output energy is at a local maximum. In the bottom left graph, the period is $\sim$2 times the pulse width and the output energy is at a local minimum. In the upper (lower) right graph, the oscillation period is $\sim$4/3 ($\sim$1) times the pulse width and again the output energy is at a maximum (minimum). Thus, it makes a big difference whether the output pulse has reached a maximum or a minimum of the oscillation in a time determined by the pulse width. As the input power is varied, the effective detuning changes due to the nonlinear frequency shift of the cavity. This, in turn, changes the effective oscillation period of the output pulse, causing the local extrema of the curves in Figs. 3(a) and 3(b).

The regime of short pulses, $\Delta\omega_{\mathrm{S}}/\Omega_{\mathrm{S}} < 1$, is thus seen to be qualitatively different from the quasi steady state regime, $\Delta\omega_{\mathrm{S}}/\Omega_{\mathrm{S}} > 1$. For short pulses, the nonlinear change of the resonance frequency relative to the *pulse* bandwidth has a significant effect on the transmission properties of the switch. For long pulses, the switching mechanism can be understood from the bistability

#149819 - $15.00 USD Received 1 Jul 2011; revised 8 Aug 2011; accepted 22 Aug 2011; published 6 Sep 2011

curve in Fig. 3(a). By increasing the input power, the transmission jumps from a small to a large value. The criterion for the bistability to occur is $\delta_S/\Delta\omega_S > \sqrt{3}/2$ [11], and therefore it is the change of resonance frequency relative to the *cavity* linewidth, which is important for the transmission in the quasi steady state regime.

Here, we have investigated the single pulse case in order to understand the more complicated case of de-multiplexing. However, single pulse transmission is also relevant for regeneration applications, where the S-shaped transfer function is used to improve the signal properties, [15]. In this case, the pulse shape changes seen in Fig. 3(c) need to be considered in detail.

4. Demultiplexing of a Data Signal

Since we are ultimately interested in the performance of switches in high speed data transmission systems, it is crucial to consider its operation on a sequence of pulses. For a demultiplexing application, the target signal pulse should be transmitted in the presence of a control pulse, while its transmission should be as small as possible in the absence of the control. The optical demultiplexing is necessary due to the limited response time of the electronics in the receiver. Here, and in Sec. 5 we will take as an example a detector with a response time of 80 ps corresponding to a bandwidth of 12.5 GHz. The total OTDM bandwidth that we will consider is 125 GHz, which corresponds to 10 channels. The detector thus integrates over 10 bit periods, and the decision between "0" or "1" is based on the amount of energy carried by the signal over the integration period. To avoid having to test all the possible bit sequences, we focus on a worst case scenario, where the difference in energy arriving at the detector in the "0" and "1" case is minimal. The maximum received energy in the case of a "0" occurs when the following 9 bits of the OTDM signal are all "1"s. This is shown in Fig. 4(a) and we denote this energy $U_{\mathrm{outS}}^{0\{1\}}$.

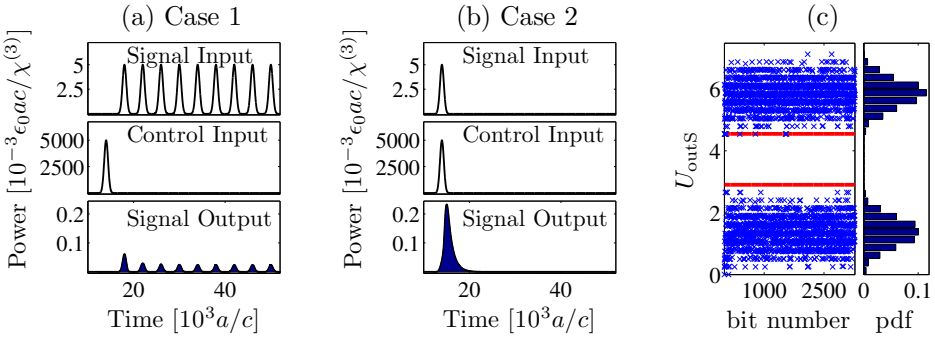

Fig. 4. (a) The top graph shows the input signal, when the target bit slot is "0" and the following bits are all "1"s. The middle graph shows the input control pulse. The lower graph shows the corresponding signal output, and $U_{\mathrm{outS}}^{0\{1\}}$ is given by the blue area under the curve. (b) The top graph shows the input signal, when the target bit is "1" followed by 9 "0"s. The middle graph shows the control pulse. The lower graph shows the corresponding signal output, and $U_{\mathrm{outS}}^{1\{0\}}$ is the area under the curve. (c) The left graph shows the detected energy for a pseudo random binary signal consisting of $2^{15}-1$ bits. The red lines indicate the worst case scenario energies, $U_{\mathrm{outS}}^{1\{0\}}$ and $U_{\mathrm{outS}}^{0\{1\}}$. The right graph shows the corresponding probability distribution function (pdf).

The minimum received energy in the case of a "1" occurs when the following 9 bits are all "0"s. Fig. 4(b) illustrates this case, and the corresponding energy is denoted $U_{\mathrm{outS}}^{1\{0\}}$. We now introduce a figure of merit (FoM) to quantify the ability of the switch to distinguish between a "0" and

#149819 - $15.00 USD Received 1 Jul 2011; revised 8 Aug 2011; accepted 22 Aug 2011; published 6 Sep 2011

"1" bit in the signal. It is defined as the ratio between the two worst case detected energies

$$\mathrm{FoM} = \frac{U_{\mathrm{outS}}^{1\{0\}}}{U_{\mathrm{outS}}^{0\{1\}}}. \tag{6}$$

To achieve a large value of the FoM, it is important that the control pulse exits the cavity fast enough to leave the succeeding signal pulses unaffected. Otherwise, $U_{\mathrm{outS}}^{0\{1\}}$ might become large and thus decrease the FoM. This patterning effect is caused by a large lifetime of cavity mode C. To confirm the validity of using $U_{\mathrm{outS}}^{0\{1\}}$ and $U_{\mathrm{outS}}^{1\{0\}}$ to define a figure of merit, we have simulated the case of a pseudo random binary signal [9], consisting of $2^{15}-1$ bits as the input in Eqs. (1) and (2). Fig. 4(c) shows the output energy registered by the detector as a function of the bit number. The figure also shows the probability distribution function (pdf) of the detected energies. The dashed black lines in Fig. 4(c) indicate $U_{\mathrm{outS}}^{0\{1\}}$ and $U_{\mathrm{outS}}^{1\{0\}}$, and it is observed that they are, in fact, upper and lower bounds on the received energy.

We have solved Eqs. (1) and (2) to investigate how the FoM depends on the different parameters describing the system. In all calculations, the peak power of the input signal is $P_{\mathrm{inS}}^0 = 10^{-6}\ \varepsilon_0 ac/\chi^{(3)}$, which is small enough compared to the control power to have a negligible effect on the nonlinear frequency shift. The signal and control pulses have equal widths, $\Delta t_{\mathrm{S}} = \Delta t_{\mathrm{C}} = 10^3\ a/c$, constant phases, $\phi_{\mathrm{inS}}(t) = \phi_{\mathrm{inC}}(t) = 0$, the delay between them is zero, and the bit rate B is $1/(4\Delta t_{\mathrm{S}})$. The varied parameters are the detunings, the cavity linewidths, and the peak power of the control pulse P_{inC}^0. In Sec. 6, we vary the response time of the detector. This is done by varying the pulse width while keeping the bit rate at $1/(4\Delta t_{\mathrm{S}})$ and the number of OTDM channels fixed at 10. This corresponds to a variation of the signal bandwidth, and the energy-bandwidth trade-off is investigated by evaluating how much energy is required to obtain a certain FoM for each bandwidth.

The parameter values from Ref. [11] are based on a 2D calculation, so the powers and energies used here are in units of [W/m] and [J/m]. To compare with real 3D devices, we may assume that the extent of the field in the transverse plane is $\sim a$ if the structure is a slab with a thickness of some fraction of a. By choosing $a = 0.6\ \mu$m and $\chi^{(3)} = 6.5\times10^{-19}$ m^2/V^2, which corresponds to a nonlinear refractive index of $n_2 = 1.5\times10^{-17}$ m^2/W [16], we have an energy unit of $\varepsilon_0 a^2/\chi^{(3)} a = 3$ pJ, and a time unit of $10^3\ a/c = 2$ ps, giving a bit rate of 125 Gbit/s. The value of n_2 we are using is achievable in AlGaAs below half the electronic bandgap [11], in which case two photon absorption is negligible.

5. Switching Dynamics with Signal and Control Pulse

First, we consider the case of a fixed linewidth of cavity mode C, $\Delta\omega_{\mathrm{C}} = 2\Omega_{\mathrm{C}}$. The control energy U_{inC} and the linewidth of cavity mode S $\Delta\omega_{\mathrm{S}}$ is varied, while the pulse widths of the signal and control are fixed. For each $\left(U_{\mathrm{inC}}, \Delta\omega_{\mathrm{S}}\right)$, both detunings are varied in order to find the maximum FoM. Fig. 5 shows how the FoM depends on δ_{S} and δ_{C} for 4 different values of $\left(U_{\mathrm{inC}}, \Delta\omega_{\mathrm{S}}\right)$. In Fig. 5(a), the quasi steady state limit with $\Delta\omega_{\mathrm{S}}/\Omega_{\mathrm{S}} = 10$ is shown, while Fig. 5(b) gives the dependence in the short pulse regime with $\Delta\omega_{\mathrm{S}}/\Omega_{\mathrm{S}} = 0.06$. Generally, the maximum FoM occurs at a larger δ_{S} when the control energy is increased. A large control energy provides a large nonlinear frequency shift of cavity mode S, which in combination with a large signal detuning results in a large change in the signal transmission. This is the reason why the FoM may be increased by using a larger control energy. Fig. 5 also shows that there is a large qualitative difference in the dependence of the FoM on the detunings in the quasi steady state and short pulse regimes. This is expected from the results in Sec. 3. The presence of multiple extrema of the FoM as a function of δ_{S} in Fig. 5(b) is caused by the same effect as the one discussed in relation to the appearance of local extrema in Fig. 3(a). Here, we have

#149819 - $15.00 USD Received 1 Jul 2011; revised 8 Aug 2011; accepted 22 Aug 2011; published 6 Sep 2011

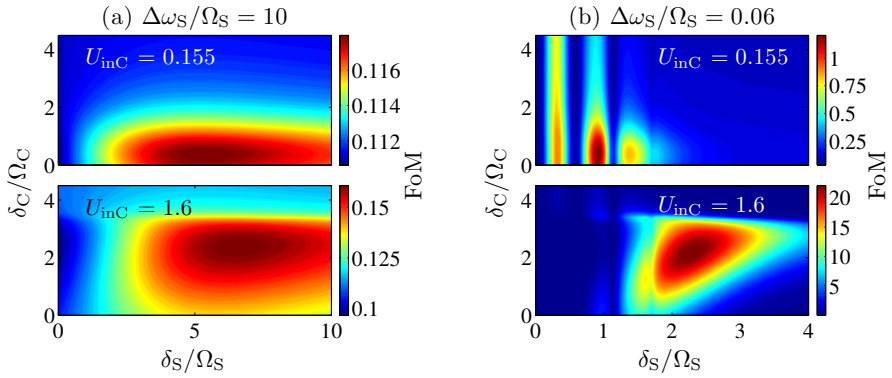

Fig. 5. (a) Variation of the FoM as a function of the signal detuning δ_S and control detuning δ_C for $\Delta\omega_S/\Omega_S = 10$ and $\Delta\omega_C/\Omega_C = 2$. The top graph corresponds to a control energy of $U_{inC} = 0.155\ \varepsilon_0 a^2/\chi^{(3)}$, while the bottom graph corresponds to $U_{inC} = 1.6\ \varepsilon_0 a^2/\chi^{(3)}$. (b) Same as (a), except the cavity linewidths are related to the pulse bandwidths by $\Delta\omega_S/\Omega_S = 0.06$ and $\Delta\omega_C/\Omega_C = 2$.

varied the detuning instead of the power as in Fig. 3(a), but it is still the oscillations in the output power that causes the extrema. A local extremum occurs for values of δ_S, where the fixed control power causes the effective oscillation period to change by $\sim$4 times the pulse width.

Another important observation, which can be made from Fig. 5, is that the FoM is much larger in the short pulse regime than in the quasi steady state case. This is also clearly illustrated in Fig. 6(a), which shows the maximum FoM as a function of U_{inC} and $\Delta\omega_S$. Notice that FoM $<$ 1 is possible, although not practically acceptable, since the energy in the denominator of Eq. (6) is an integral over 9 pulses, whereas the numerator results from an integration over 1 pulse. The

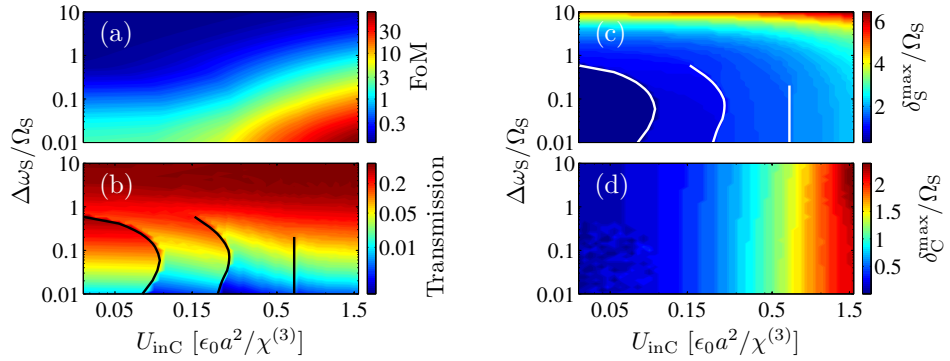

Fig. 6. (a) The maximum of the FoM found by varying (δ_S, δ_C) as a function of U_{inC} and $\Delta\omega_S$. (b) The transmission of the signal pulse, $U_{outS}^{1\{0\}}/U_{inS}^{1\{0\}}$, corresponding to the maximum of the FoM in (a). The black lines indicate discontinuity boundaries, where the transmission suddenly changes value. (c) The value of δ_S^{max}/Ω_S corresponding to the maximum of the FoM in (a). The white lines indicate discontinuity boundaries. (d) The value of δ_C^{max}/Ω_C, which corresponds to the maximum of the FoM in (a).

price to pay for the increase in the FoM is a reduction in transmission, $U_{outS}^{1\{0\}}/U_{inS}^{1\{0\}}$, which is illustrated in Fig. 6(b). The discontinuities in the transmission occur when the global maximum

#149819 - $15.00 USD Received 1 Jul 2011; revised 8 Aug 2011; accepted 22 Aug 2011; published 6 Sep 2011

of the FoM shifts from one local maximum to another in the (δ_S, δ_C)-plane, cf. Fig. 5(b). The value of the signal detuning, where the maximum in the FoM occurs, δ_S^{max}, is plotted in Fig. 6(c) and the discontinuity boundaries are indicated by the white lines. In Fig. 6(d) we show δ_C^{max} and it is observed to depend much stronger on U_{inC} than $\Delta\omega_S$. Since the signal power is too small to shift the resonance frequency of cavity mode C, it makes sense that $\Delta\omega_S$ does not have a significant influence on δ_C^{max}. The maximum in the control detuning increases with increasing control energy because a larger power causes a larger shift of ω_C and in order to get a maximum amount of power in the cavity δ_C^{max} must also increase.

Many of the tendencies observed in Figs. 6(a)-(c) may be understood from the solution of Eq. (1) in the linear limit. For a single Gaussian input pulse, the output energy is given by

$$U_{outS} = P_{inS}^0 \Delta t_S \frac{\pi}{4} X e^{\ln(2)(X-i2Y)^2} \left(\mathrm{Erfc}\left[\sqrt{\ln(2)}(X-i2Y)\right] + e^{i8\ln(2)XY}\mathrm{Erfc}\left[\sqrt{\ln(2)}(X+i2Y)\right]\right), \quad (7)$$

where

$$X = \frac{\Delta\omega_S}{\Omega_S}, \quad Y = \frac{\delta_S}{\Omega_S}, \quad \text{and} \quad \mathrm{Erfc}(z) = 1 - \frac{2}{\sqrt{\pi}}\int_0^z e^{-t^2} dt.$$

From the definition of the FoM in Eq. (6) and the fact that the control power effectively changes δ_S, cf. Eq. (4), it seems reasonable to expect that the optimum value of δ_S/Ω_S is found close to a maximum of the relative change of U_{outS} with respect to δ_S/Ω_S

$$\partial U_{outS}^{rel}(\delta_S/\Omega_S) = \left| \frac{dU_{outS}}{d(\delta_S/\Omega_S)} \right| \frac{1}{U_{outS}}. \quad (8)$$

In Fig. 7(a) we have plotted the maximum of $\partial U_{outS}^{rel}(\delta_S/\Omega_S)$ as a function of $\Delta\omega_S/\Omega_S$. The ob-

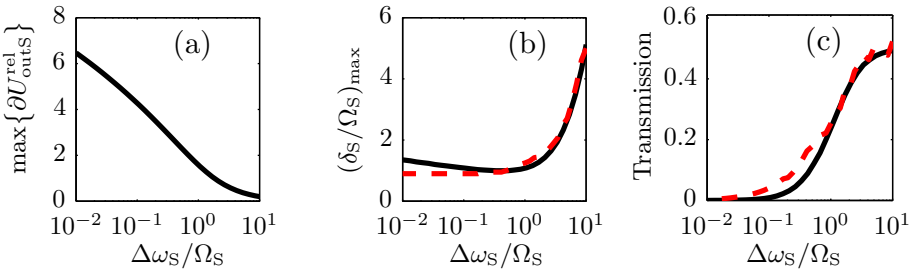

Fig. 7. (a) The maximum value of $\partial U_{outS}^{rel}(\delta_S/\Omega_S)$, defined in Eq. (8), plotted as a function of the bandwidth ratio between the pulse and the cavity. (b) The value of δ_S/Ω_S where the maximum in (a) occurs (solid black) and a cross section of δ_S^{max}/Ω_S at $U_{inC} = 0.105\ \varepsilon_0 a^2/\chi^{(3)}$ from Fig. 6(c) (dashed red). (c) The transmission corresponding to the maximum in (a) (solid black) and a cross section of the transmission at $U_{inC} = 0.105\ \varepsilon_0 a^2/\chi^{(3)}$ from Fig. 6(b) (dashed red).

served increase in $\max\{\partial U_{outS}^{rel}\}$ as $\Delta\omega_S$ is decreased thus explains why the FoM also increases when $\Delta\omega_S$ is decreased, as it is seen in Fig. 6(a). A more intuitive way to understand this behavior in the short pulse regime, is to consider the transient oscillations resulting from a step function input given in Eq. (5). As $\Delta\omega_S$ is decreased, the ratio between the maxima and minima of the oscillations as well as the cavity lifetime increase, which causes a larger difference in the output energy between the upper and lower pulses in Fig. 3(c). This means that the change in output energy due to the presence of the control pulse increases as $\Delta\omega_S$ is decreased.

#149819 - $15.00 USD Received 1 Jul 2011; revised 8 Aug 2011; accepted 22 Aug 2011; published 6 Sep 2011

Fig. 7(b) shows the value of δ_S/Ω_S, where the maximum in ∂U^{rel}_{outS} occurs (solid black curve) and a cross section of δ^{max}_S/Ω_S from Fig. 6(c) at $U_{inC} = 0.105\ \varepsilon_0 a^2/\chi^{(3)}$ (dashed red curve). The agreement between the curves is seen to be good for large values of $\Delta\omega_S$, but there is a discrepancy when the cavity linewidth decreases. This is also the case for the transmission corresponding to the maximum of ∂U^{rel}_{outS}, which is plotted in Fig. 7(c) (solid black curve) along with a cross section of the signal transmission, $U^{1\{0\}}_{outS}/U^{1\{0\}}_{inS}$, at $U_{inC} = 0.105\ \varepsilon_0 a^2/\chi^{(3)}$ from Fig. 6(b) (dashed red curve). The reason for this discrepancy is that the denominator in Eq. (6) is an integration over 9 bits. When $\Delta\omega_S$ decreases, the signal energy in one bit does not escape the cavity before the next pulse arrives. This gives rise to a much more complicated behavior, which can not be accounted for by an analysis based on a single pulse input. The discontinuities in Fig. 6(a)-(c) are not described by the linear analysis either. These can only be understood as an interplay between the nonlinear frequency shift and the transient oscillations of the output pulses observed in Fig. 3(c). This conclusion is supported by the fact that the discontinuities appear in the short pulse regime, where the oscillations were observed in Fig. 3(c). Even though the linear analysis is not able to describe all the details of Fig. 6(a)-(c), it is still very useful for understanding the general trends.

From Figs. 6 and 7 we have learned that decreasing the bandwidth of cavity mode S provides a large figure of merit, but at the cost of a reduction in transmission. Here, we will use a lower bound on the transmission of 0.1, corresponding to a cavity linewidth of $\Delta\omega_S \sim \Omega_S/3$, or equivalently, a quality factor of, $Q_S \sim 2500$. Fig. 6(a) also shows that to achieve a figure of merit well above 1 with this cavity linewidth, we must use larger control energies.

Using a fixed value of $\Delta\omega_S = \Omega_S/3$, we now vary the control energy and the linewidth of cavity mode C in the same way as in Fig. 6. The results are given in Fig. 8(a)-(d). From Fig. 8(a)

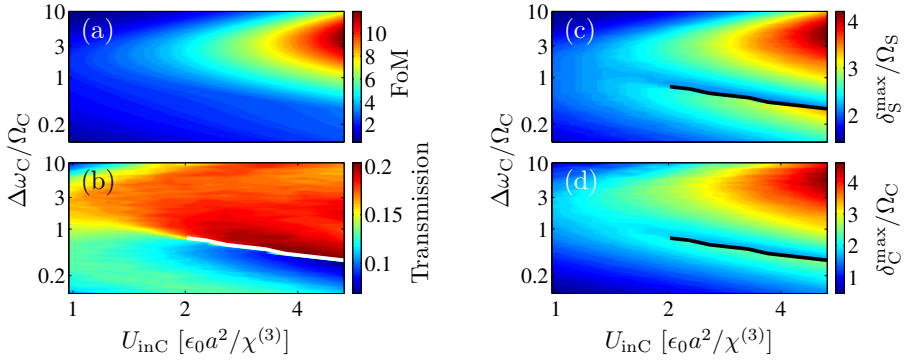

Fig. 8. (a) The maximum FoM found by varying (δ_S, δ_C) as a function of U_{inC} and $\Delta\omega_C$. (b) The transmission of the signal, $U^{1\{0\}}_{outS}/U^{1\{0\}}_{inS}$, corresponding to the maximum of the FoM in (a). As in Fig. 6(b), the white line indicates a discontinuity boundary, where the transmission suddenly changes value. (c) The value of δ^{max}_S/Ω_S corresponding to the maximum of the FoM. The discontinuity boundary is also shown with a black line. (d) The value of δ^{max}_C/Ω_C, which corresponds to the maximum of the FoM along with the discontinuity boundary.

it is observed that there is an optimum value of $\Delta\omega_C$, which minimizes the required control energy to achieve a certain value of the figure of merit. If the cavity linewidth is large, the field enhancement inside the cavity is small, and thus it requires a larger input power to achieve a certain frequency shift. On the other hand, if the linewidth becomes smaller, the figure of merit is reduced by patterning effects as mentioned in Sec. 4. Fig. 8(b) shows the dependence of the

#149819 - $15.00 USD Received 1 Jul 2011; revised 8 Aug 2011; accepted 22 Aug 2011; published 6 Sep 2011

signal transmission, $U_{\mathrm{outS}}^{1\{0\}}/U_{\mathrm{inS}}^{1\{0\}}$. Like in Fig. 6(b), a discontinuity is also observed here and is indicated with a white curve. Again, it is caused by the global maximum of the FoM shifting from one local maximum to another.

The values of detuning, which correspond to the maximum in the FoM, are depicted in Figs. 8(c) and 8(d). It is clearly seen from these graphs that the discontinuity in Fig. 8(b) corresponds to a discontinuous change in $\delta_{\mathrm{S}}^{\max}$ and $\delta_{\mathrm{C}}^{\max}$. By comparing Figs. 8(a) and 8(c) it is observed that the maximum in the FoM is coincident with a maximum in δ_{S}. This makes sense because the difference between the numerator and denominator in Eq. (6) can be made larger by using a larger detuning if sufficient control power is available to deliver a correspondingly large frequency shift. From Fig. 8(d) it is observed that the behavior of $\delta_{\mathrm{C}}^{\max}$ closely resembles that of $\delta_{\mathrm{S}}^{\max}$. It is to be expected that $\delta_{\mathrm{C}}^{\max}$ is the value of δ_{C}, where a maximum amount of control power is available to shift the resonance frequency of cavity mode S. This is the reason for the increase in $\delta_{\mathrm{C}}^{\max}$ with U_{inC}, because the shift of ω_{C} also increases with control power.

6. Energy-Bandwidth Trade-Off

From Fig. 8(a), we have learned that there is an optimum ratio between the linewidth of cavity mode C and the spectral width of the pulse, which results in a minimum in the control energy required to achieve a given value of the FoM. To quantify the energy-bandwidth trade-off, we now vary the linewidth $\Delta\omega_{\mathrm{C}}$ and control energy as in Fig. 8 for different values of the two pulse widths, $\Delta t_{\mathrm{S}} = \Delta t_{\mathrm{C}}$. The bit rate is still given by $1/(4\Delta t)$, so this allows us to investigate the dependence of the minimum required control energy on the bit rate of the signal. We keep the ratio $\Delta\omega_{\mathrm{S}}/\Omega_{\mathrm{S}}$ fixed at 1/3 to get sufficient transmission, cf. Sec. 5. The result is shown in Fig. 9(a). The different curves correspond to the minimum energy required to achieve different values of the FoM. It is clearly observed how the energy requirement increases as the bit rate

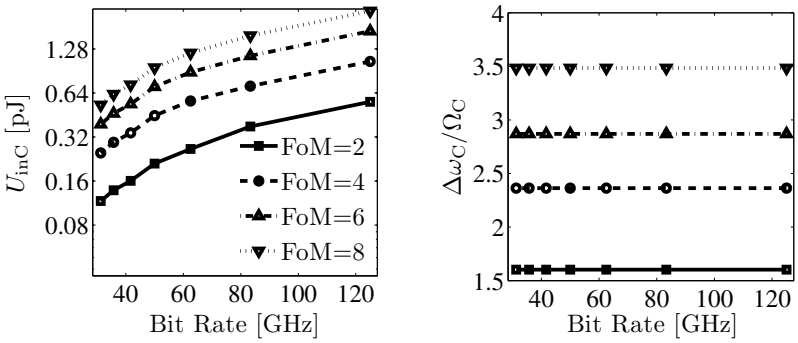

Fig. 9. (a) Minimum required control energy to obtain different values of the FoM (indicated by the different curves) as a function of the signal bit rate. (b) The ratio of the linewidth of cavity mode C and the pulse spectral width corresponding to the minimum energies shown in (a). The diferent curves correspond to the same values of the FoM as in (a). In both (a) and (b), the parameter values from Sec. 4 have been used.

increases, and as the value of the FoM increases. Fig. 9(b) shows the optimum ratio, $\Delta\omega_{\mathrm{C}}/\Omega_{\mathrm{C}}$, corresponding to the minimum in U_{inC}. The different curves correspond to the same values of the FoM as in Fig. 9(a). The optimum ratio is seen to be independent of the bit rate, but increases as the value of the FoM is increased. Since the bit rate is varied by changing Ω_{C}, we see that the optimum linewidth of cavity mode C changes, corresponding to a quality factor of $Q_{\mathrm{C}} \approx 900$ for $B = 40$ GHz and $Q_{\mathrm{C}} \approx 300$ for $B = 125$ GHz, when $\Delta\omega_{\mathrm{C}}/\Omega_{\mathrm{C}} \approx 3$. For a bit rate of 125 GHz, the quality factors of the two modes, Q_{S} and Q_{C}, differ by a factor of 9. As explained in Sec. 2,

#149819 - $15.00 USD Received 1 Jul 2011; revised 8 Aug 2011; accepted 22 Aug 2011; published 6 Sep 2011

such a large difference is easy to achieve in a structure with spatially separated waveguides, like the one shown in Fig. 1(a), suggesting that such structures are advantageous when operating at high bit rates.

7. Conclusion

Using a coupled mode theory we have studied the performance of all-optical photonic crystal microcavity switches. For ultra high bandwidth signals employing very short pulses, our analysis show that the transmission properties are closely related to the change in resonance frequency relative to the pulse bandwidth and interference effects play a major role. This shows that the bistability curves obtained by a steady analysis can not be used to understand the switching dynamics if the pulse width is small compared to the cavity lifetime.

The introduction of a figure of merit (FoM) based on the detection of a demultiplexed OTDM signal allows us to quantify the energy-bandwidth trade-off and thereby define the minimum required switching energy in a way that is suitable for applications in high speed optical communication systems. Furthermore, the FoM applies to any type of switching device and can therefore be used in a performance comparison between different systems.

The definition of the FoM in Eq. (6) takes into account the detrimental patterning effects, which are caused by the cavity lifetime. The relatively small optimum value of 300 for Q_C at $B = 125$ GHz shows that these effects are dominant in the energy-bandwidth trade-off compared to the field enhancement caused by the cavity at high bit rates. This conclusion underlines the importance of using realistic data signals consisting of many bit periods to estimate the performance of switching devices.

Besides providing new insights into the physical mechanisms of the switching operation, our numerical investigation also predicts parameter ranges where optimal performance is predicted. These results should be useful for the design and analysis of high performance all-optical photonic crystal microcavity switching devices.

Acknowledgments

The authors acknowledge financial support from Villum Fonden via the NATEC (NAnophotonics for TErabit Communications) Centre, as well as from EU FP7 via the COPERNICUS Project. The authors would also like to thank Christophe Peucheret and Jing Xu for fruitful discussions.

#149819 - $15.00 USD Received 1 Jul 2011; revised 8 Aug 2011; accepted 22 Aug 2011; published 6 Sep 2011